Comparison of solid oxide fuel cell (SOFC) electrolyte materials for operation at 500 °C

Jun Zhang[1*], Christian Lenser[1], Norbert H. Menzler[1], Olivier Guillon[1, 2]

[1] Forschungszentrum Jülich GmbH, Institute of Energy and Climate Research, Materials Synthesis and Processing (IEK-1), Jülich, Germany

[2] Jülich Aachen Research Alliance: JARA-Energy, 52425 Jülich, Germany

Abstract

Solid oxide fuel cells (SOFCs) operating at low temperature (~ 500 °C) enable new fields of application, such as auxiliary power units (APUs) or power generation for mobile applications. However, the state-of-the-art electrolyte material currently used in intermediate-temperature SOFCs (yttria-stabilized zirconia (YSZ)) does not provide sufficiently high ionic conductivity for low temperature applications. When looking for alternatives, the conductivity values for each material found in widely-cited literature can be confusing, as the reported values are sometimes in conflict with each other. Therefore, we present a systematic comparison of the conductivity of the three most popular, commercially available electrolyte materials, i.e. YSZ, scandia-stabilized zirconia (ScSZ), and gadolinium-doped ceria (GDC). By using electrochemical impedance spectroscopy (EIS) to characterize the ionic conductivities, we find that at 500 °C, GDC has a higher ionic conductivity (5.8×10^{-3} S·cm^{-1}) than ScSZ (2.5×10^{-3} S·cm^{-1}) and YSZ (1.1×10^{-3} S·cm^{-1}). The properties of the starting powders, powder processing and the microstructure after sintering were taken into account. This conductivity comparison can be used as a guide when deciding on electrolyte materials for different SOFC applications, especially when the fabrication of different thickness of the electrolyte layer has to be considered, and rectify misleading information in the literature.

1. Introduction

Solid oxide fuel cells (SOFCs) convert the chemical energy in a variety of fuels (H_2, CH_4 or higher hydrocarbons) into electricity with lower greenhouse gas emissions and higher electrical efficiency compared to traditional combustion engines or other fuel cell types. The high operation temperature (~ 900 °C) of electrolyte supported SOFCs limits their further commercialization. With the development of the anode-supported SOFCs (AS-SOFC), which allows the cell to be fabricated with a much thinner electrolyte in comparison to the electrolyte-supported cells, the operation temperatures can be lowered to the range of 700 – 800 °C while still providing improved power densities. The AS-SOFCs fabricated at Forschungszentrum Jülich, for example, using 1 µm 8YSZ (8 mol% Y_2O_3 doped ZrO_2) electrolyte, have demonstrated a high single cell performance at 700 °C (> 1 W/cm^2 at 0.7 V, using humidified hydrogen as fuel and laboratory air as oxidant) [1]. Another one with 10 µm 8YSZ electrolyte also shows excellent

* Corresponding author.
E-mail address: jun.zhang@fz-juelich.de (J. Zhang)

stability (> 80,000 hours operation time) at 700 °C [2]. In addition, good power density and long-term operation of SOFCs are also reported by other researchers [3-7].

There is a growing interest to lower the operation temperature of SOFCs further to ~ 500 °C to enable other applications, such as auxiliary power unit applications (APUs) or power generation for mobile applications [8, 9]. However, the state-of-the-art electrolyte configuration (~ 10 µm YSZ) used in the intermediate temperature SOFC (IT-SOFC) does not provide a sufficiently high ionic conductivity to reach acceptable area specific resistance from the electrolyte (ASR_{el}) at low temperatures [10].

The ASR_{el} can be calculated via [11]:

$$ASR_{el} = L \cdot \sigma^{-1} \tag{1}$$

where L is the thickness of the electrolyte and σ is the oxygen ionic conductivity. Resulting from this equation, two strategies are commonly applied to reduce the ASR_{el}. The first one is to reduce the thickness of the YSZ electrolyte further. The power density *P* of an SOFC can be calculated according to:

$$P = \frac{V^2}{(ASR_{el}+ASR_A+ASR_C)} \tag{2}$$

where *V* is the cell voltage and ASR_{el}, ASR_A and ASR_C are the area-specific resistance of electrolyte, anode and cathode, respectively. Since the electrode resistance can be expected to be larger than the electrolyte resistance at such low temperature, a value of ASR_{el} = 0.1 Ω/cm^2 should not be exceeded if a power density of 1 W/cm^2 is targeted for the SOFC operated at 500 °C. Accordingly, an electrolyte with thickness around 1 µm would be required for the operation of a SOFC using YSZ as the electrolyte [10, 13]. While thin YSZ electrolytes in AS-SOFC have been demonstrated by different researches[14], for example by using chemical vapor deposition (CVD)[15], pulsed laser deposition (PLD)[16], physical vapor deposition (PVD)[17] or sol-gel routes [18], the scale-up of these techniques to industrial application level still remains a challenge due to the extremely high surface quality of the anode support that is necessary to grow/deposit a dense electrolyte layer.

The second strategy is to replace YSZ by other materials with higher conductivity. Electrolyte materials that offer higher ionic conductivities than that of YSZ are listed in Table 1.

Table 1 Comparison of total conductivity values for different electrolyte materials at 500 °C (with calculated required thickness based on an ASR_{el} = 0.1 Ω cm^2)

Electrolyte material	Ionic conductivity (S cm^{-1})	Required thickness (µm)	Reference
$(Y_2O_3)_{0.08}(ZrO_2)_{0.92}$	1.1×10^{-3}	1.1	[19]
$(BiO_{1.5})_{0.88}(DyO_{1.5})_{0.08}(WO_3)_{0.04}$	9.8×10^{-2}	98	[20]
$Ce_{0.9}Gd_{0.1}O_{1.95}$	6.3×10^{-3}	6.3	[21]
$(Sc_2O_3)_{0.08}(CeO_2)_{0.01}(ZrO_2)_{0.91}$	4.9×10^{-3}	4.9	[22]
$La_{0.9}Sr_{0.1}Ga_{0.9}Mg_{0.1}O_3$	6.0×10^{-3}	6.0	[23]

However, a high ionic conductivity is not the only requirement for the material to serve as the electrolyte in AS-SOFCs. Properties such as chemical compatibility with electrodes at high temperatures or chemical stability in both oxidizing and reducing atmospheres have to be considered when choosing the electrolyte for an SOFC[24]. For example, though Bi_2O_3-based oxides are reported to have a much higher ionic conductivity than other electrolyte materials (for example, the $(BiO_{1.5})_{0.88}(DyO_{1.5})_{0.08}(WO_3)_{0.04}$ in Table 1), they reduce to metallic Bi under a reducing atmosphere and undergo a transformation to a low ionic conductive phase at the operation temperatures [25, 26]. Similarly, $LaGaO_3$-based electrolytes, such as $La_{0.9}Sr_{0.1}Ga_{0.9}Mg_{0.1}O_3$, also have an outstanding ionic conductivity, but they react with nickel at operation temperatures, which is commonly used as the state-of-the-art anode material, to form a highly resistive phase[27]. Gd-doped ceria (GDC) exhibits mixed ionic and electronic conductivity (MIEC) under reducing atmosphere, but it has already been shown that the degree of electronic conductivity in GDC is highly temperature dependent[9]. Therefore, GDC should be suitable for operation temperatures below 650 °C [28-30]. Scandia-stabilized zirconia (ScSZ) shows a phase transition from the high-conductivity cubic phase to a low-conductivity tetragonal phase during cooling or aging at high temperatures (1250 – 1550 °C)[31]. Nevertheless, doping of Ce into ScSZ is reported to stabilize the cubic phase in all SOFC operation temperatures [32-34].

Despite the fact that the electrical performance of YSZ, ScSZ and GDC has been broadly investigated [9, 10, 13, 35-38], the conductivity values presented in some widely cited literature are scattered. For example, in the review article by Brett et al. [9], ScSZ has nearly the same ionic conductivity as GDC at 500 °C and even has a superior conductivity than GDC at temperatures lower than 500 °C, while the conductivities of both GDC and ScSZ given as significantly larger than that of YSZ at all temperatures. In contrast to this, in review [13], ScSZ has a lower conductivity than GDC at temperature of 500 °C and below. Moreover, in this review [13], the conductivity of ScSZ is similar to that of YSZ at lower temperatures (lower than 450 °C). On the other hand, Kumar et al. suggest that ScSZ exhibits much higher oxygen-ion conductivity than 8YSZ, and thus has a potential to be utilized as an electrolyte for low temperature SOFC.[22] Similar expression can also be seen in some other publications [39, 40]. Citing an overview article by Mahato *et* al.,[41] Thommy *et* al. state that "Gadolinium-doped ceria $Ce_{0.9}$ $Gd_{0.1}O_{1.95}$ (CGO) appears as a good candidate for such an application since it presents at 600 °C the same level of conductivity as the benchmark electrolyte YSZ at 900 °C." This is a vast overstatement, but illustrates the false impressions that can arise from conflicting literature information. Also, for the more frequently investigated intermediate or high temperature range (> 650 °C), confusing data exists for the conductivity comparison, as shown in Table 2.

Table 2 Conductivity comparison for YSZ, ScSZ and GDC from different literature sources (data is approximated from plots in each reference).

materials	Conductivity (S cm^{-1}) at specific temperature		reference
	500 °C	700 °C	
YSZ	7.2×10^{-4}	8.4×10^{-3}	
ScSZ	9.6×10^{-3}	5.5×10^{-2}	[9]
GDC	8.8×10^{-3}	7.3×10^{-2}	
YSZ	8.2×10^{-4}	--	
ScSZ	1.6×10^{-3}	--	[13]
GDC	5.7×10^{-3}	--	
YSZ	--	3.0×10^{-2}	
ScSZ	--	--	[42]
GDC	5.9×10^{-3}	4.4×10^{-2}	
YSZ	9.1×10^{-4}	1.2×10^{-2}	
ScSZ	--	--	[10]
GDC	1.5×10^{-2}	7.4×10^{-2}	
YSZ	3.4×10^{-3}	5.5×10^{-3}	
ScSZ	--	--	[5]
GDC	7.8×10^{-3}	1.8×10^{-2}	
YSZ	1.0×10^{-3}	1.8×10^{-2}	
ScSZ	2.4×10^{-3}	5.3×10^{-2}	This work
GDC	5.9×10^{-3}	4.3×10^{-2}	

There are two points that need to be considered with regards to the conductivity presented in the aforementioned reviews. First, all of them use data referenced from other literature or reviews. For example, conductivity data from review [9] are referenced from review [43] and references therein. However, the conductivity data in review [43] are referenced to review [44], in which we can't find the actual conductivity data. In much the same way, the data from review [13] were calculated from the center of the mass of the conductivity values from reviews [5] and [36]. This is, of course, a valid strategy when writing a review, but does present the danger of error propagation. Second, details about the property of the starting powders, the processing of the powders and the microstructure after sintering, which influence the ionic conductivity, is often missed in the aforementioned reviews and their referenced sources provided. For example, Mori et al. investigated the effects of the morphology of the starting

powders and they found that $Sm_{0.2}Ce_{0.8}O_{1.9}$ sintered from round-shaped particle had higher conductivity than that sintered from elongated particles, and they explained this by the micro-domain size effects [45]. Furthermore, Chen studied the effects of the sintering condition and found that YSZ sintered at 1350 °C for 4 h had a lower conductivity (0.105 S cm^{-1}) compared to the one sintered at 1250 °C for 8 h (0.112 S cm^{-1}). The explanation for the results is the variation of relative density and grain size[46]. Besides those effects, the level of impurities in the material is crucial, especially the content of SiO_2, which segregates to the grain boundary to cause a larger grain boundary resistance and therefore imposes deleterious effects on the ionic conductivity [30, 47]. While the aforementioned reviews note the role of these effects, they are very hard to present concisely in a review.

It is true that there is no material that can completely fulfill all the desired criteria, including high ionic conductivity, better compatibility with the electrodes and stability under reducing atmosphere or during operation, all at once. However, the interest in YSZ, GDC and ScSZ is still high since these materials show a promising (or compromised) mix of those criteria. In this paper, we compare the ionic conductivities of widely used YSZ, GDC and ScSZ that are commercially available in SOFC industries. By examining their properties from the starting powders and sintering the material to similar high relative density ceramics, the effect of microstructure to ionic conductivity can be minimized. We aim to provide accurate and reliable conductivity values for these ceramics made from commercially available powders. Furthermore, a model based on the obtained conductivities was developed for understanding how the grain size would affect ASR_{el} when different thickness of electrolyte is used in a SOFC.

2. Background

The temperature dependence of the ionic conductivity is commonly presented in an Arrhenius equation:

$$\sigma \mathrm{T} = \sigma_0 exp^{-\frac{Q}{kT}} \tag{2}$$

where σ, T, σ_0, Q, k denote the ionic conductivity, temperature, pre-factor of the ionic conductivity, activation energy and the Boltzmann constant, respectively. According to the equation, if plotting the equation in the form of "ln σT vs 1/T", the relationship should be linear. However, it is common to see a change of the slope (the activation energy) in many reports [20, 39, 48, 49].

A common interpretation of this is based on a three-stage model of conductivity in doped conductors:[50] in the high-temperature (intrinsic) regime, the charge carrier density n is dominated by self-ionization and therefore increases exponentially with T. In the intermediate regime, n is constant and determined by the dopant concentration, while in the low temperature range, associated defect pairs are formed due to the Coulomb interaction between the negatively-charged dopant cations and positively-charged oxygen vacancy. A temperature-dependent fraction of oxygen vacancies is thereby "trapped" and thus the "mobile" oxygen vacancies concentration is lowered. At sufficiently low temperature, the apparent activation energy Q is a superposition of the migration enthalpy for ionic motion H_m and the association enthalpy H_s for the dissociation of the defect dipoles. At sufficiently high temperature, the "trapped" vacancies become mobile and then Q is equal to the migration enthalpy H_m.

Kilner and Steele explicitly state that this model only applies to dilute dopant concentrations[50]. However, values of the association enthalpy H_{ass} on the order of a few tenth of an eV are frequently reported, while the corresponding transition temperatures usually reported below 600 °C. [39, 51-54] From Boltzmann statistics alone, such high values for H_{ass} do not match such low transitions temperatures, since the exponential expression yields very small values unless *H* and *kT* are similar in magnitude. Correspondingly, Nowick and Park demonstrated that the break temperature (which they define as the temperature where the amount of associated and free vacancies are equal, i.e. the transition between predominantly associated and free vacancies) should be expected well above 1000°C in oxide with several mole-% of dopants and association enthalpies on the order of 0.3 eV [55]. For these and other reasons, Nowick and Park therefore argue that the conductivity of doped oxides is always in the "association regime" at temperatures relevant for SOFC operation (i.e. below 1000 °C). The bending in the "*ln σT – 1/T*" plots therefore cannot be described as the transition from trapped to free vacancies.

Recently, Ahamer et al. provided an approach to explain the changing slope in the Arrhenius plot of the temperature-dependent conductivity of YSZ. They suggested that a material has a series connection of regions that each has different conductivities. In other words, different conduction pathways exist for oxygen vacancies with different barrier heights, which have to be passed (or jumped) along an average path. These different barrier heights refer to the fact that the potential energy landscape around an oxygen vacancy is strongly influenced by the amount of dopant ions around the vacancy site, and that the activation barrier will be different based on whether a start site or finish site of a jump is located next to Ce^{4+} ions or Gd^{3+} ions (in the case of GDC). While the common observed two different activation energy in some electrolyte materials for SOFC at high and low temperature indicates two parallel conduction pathways, or two barrier heights, called the ''two barrier model'', which can be presented as following: [56]:

$$\sigma T = \left(\frac{1}{\gamma_1 e^{-E_{a,1}/kT}} + \frac{1}{\gamma_2 e^{-E_{a,2}/kT}} \right)^{-1} \tag{3}$$

where $E_{a,1}$ and $E_{a,2}$ are the two barrier heights and γ_i equals to $\frac{Z^2 e_0^2 a_0^2 n_{V,tot} v_i^0}{k\beta_i}$(where z denotes the absolute charge, e_0 the elementary charge, a_0 the average jump distance, $n_{v,tot}$ the total vacancy concentration, v_i^0 is a pre-factor that includes the attempt frequency, migration entropy and correlation effects), k is Boltzmann's constant and β_i a weight factor of successful jumps across barrier heights $E_{a,i}$). As for this study, a similar bending behavior of the activation energy is also observed when we compare the ionic conductivity, therefore, the ''two barrier model'' will be applied for the analysis.

3. Experimental

Commercially available $(Y_2O_3)_{0.08}(ZrO_2)_{0.92}$ (YSZ) (TZ-8Y, Lot No. Z803541P, TOSOH, Japan), $Gd_{0.1}Ce_{0.9}O_{1.95}$ (GDC) (GDC10-HP, Lot No. CB080, Fuelcellmaterials, USA) and $(Sc_2O_3)_{0.1}(CeO_2)_{0.01}(ZrO_2)_{0.89}$ (ScSZ) (10Sc1CeSZ-R2, Lot No. J2728 DKKK, Japan) powders were used directly for the studies. The impurity level was checked by inductively coupled plasma optical emission spectroscopy (ICP-OES) using a spectrometer (iCAP7600, Thermo Scientific). The dilatometer experiments were conducted in a push-rod vertical dilatometer (TMA 402, NETZSCH) for monitoring the in situ shrinkage of the sample and the sample was

prepared by pressing the powder into pellets of 8 mm in diameter and 10 mm in height by using a steel die at a pressure of 150 MPa. The sample used for ionic conductivity was made by pressing powder to to make discs of ~ 13 mm in diameter and ~ 3 mm in thickness by using a steel die at a pressure of 150 MPa, and then the resulting compacts were sintered in air at 1400 °C with a dwell time of 2 hours using a heating rate of 3 K/min and then a cooling rate of 5 K/min to room temperature. The ionic conductivity measurements were then conducted as a function of temperature in air using an impedance analyzer (Alpha-A High performance Frequency Analyzer, Novocontrol Technologies GmbH, Germany) with frequency ranged from 0.1 Hz to 1 MHz. A thin (~ 15 nm) Platinum layer was sputtered on both polished surfaces of the sintered pellets, followed by additional hand brushing of Pt paste to serve as electrodes. The coated samples were then fired at 900 °C for 2 h in air to provide good bonding between the Pt electrode and ceramic samples. The impedance data were collected during the cooling process from 800 °C to room temperature with a dwell-time of 2 hours to reach thermal equilibrium at each measured temperature. The impedance data were analyzed using "Zview 3.2". The corresponding stray capacitances (under open circuit condition) of the setup, which arose from nonideal shielding of the wiring and the electrodes, were determined to around 5 pF. The microstructure investigation of the powders and sintered pellets were conducted using a scanning electron microscope (SEM) (ZEISS ULTRA 55, Oberkochen, Germany) equipped with an energy-dispersive X-ray spectroscopy (EDX) system (Oxford X-Max, Oxford Instruments- Wiesbaden, Germany). Sintered samples were first polished and then thermally etched by annealing at 100 °C under the sintering temperature for 1 h in order to clearly observe and evaluate the grain size and porosity. For each ceramic, around 1500 grains were analyzed by the software "analySIS pro" to determine the average grain size. For the sintering behavior and ionic conductivity measurements, three identical pellets were made for each material to ensure the reproducibility of the measurements and to calculate the corresponding standard deviations.

4. Results and discussion

4.1 Powder property characterizations

The impurity levels of the three powders were checked and are compared in none of the powders showed hard agglomeration, while GDC has a little higher degree of sintered agglomerates of primary particles than YSZ and ScSZ. The primary particle size observed from SEM in Figure 1, shows GDC has the smallest primary particle size (less than 50 nm), followed by YSZ (around 100 nm) and ScSZ (a little higher than YSZ).

Table 3, confirming that each powder is highly pure, especially with extremely low Si contents. Therefore, it can be expected that the impurities have a negligible effect on the ionic conductivities. In addition, the powder morphologies were also examined before sintering. As shown in Figure 1, none of the powders showed hard agglomeration, while GDC has a little higher degree of sintered agglomerates of primary

particles than YSZ and ScSZ. The primary particle size observed from SEM in Figure 1, shows GDC has the smallest primary particle size (less than 50 nm), followed by YSZ (around 100 nm) and ScSZ (a little higher than YSZ).

Table 3 Impurity content in the commercial powder.

powder	Elements content (ppm)			
	Si	Co	Fe	Cu
YSZ	24 ± 6	52 ± 4	38 ± 17	40 ± 20
ScSZ	19 ± 6	47.3 ± 1.0	31 ± 6	30 ± 20
GDC	21 ± 1.4	<1	37 ± 4	51.7 ± 0.7

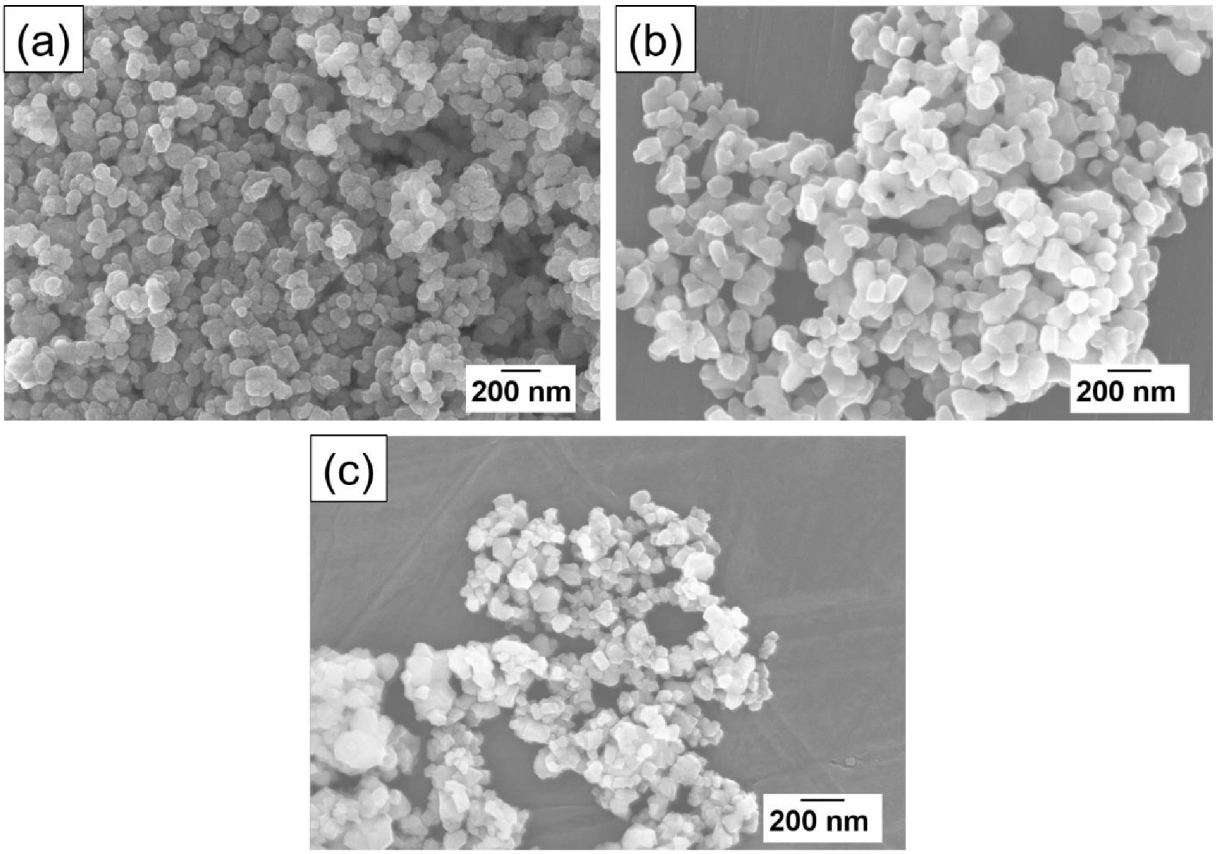

Figure 1: Powder morphologies observed by SEM for (a) YSZ, (b) ScSZ and (c) GDC

4.2 Dilatometry

The sintering behavior of these three materials were checked by dilatometry, as shown in Figure 2. All of these three materials show a comparable one-step sintering behavior. They start to shrink around 900 °C (ScSZ shrinks at a little higher temperature, around 1000 °C), which is reached after 300—320 min, with the chosen heating rate. But the shrinkage slow down at different temperatures, 1300 °C for YSZ, 1400 °C for ScSZ and GDC. In addition to that, GDC has a smaller shrinkage compared to YSZ and ScSZ. The reason for that might be that GDC already has a higher relative green density before sintering. The relative green density for YSZ, ScSZ and GDC is 45.3%, 43.6% and 57.2%, respectively. All these values testify the high quality of the powders and their good sinter ability. Therefore, based on the dilatometry measurement, a sintering temperature of 1400 °C for 2 hours was chosen for all three materials.

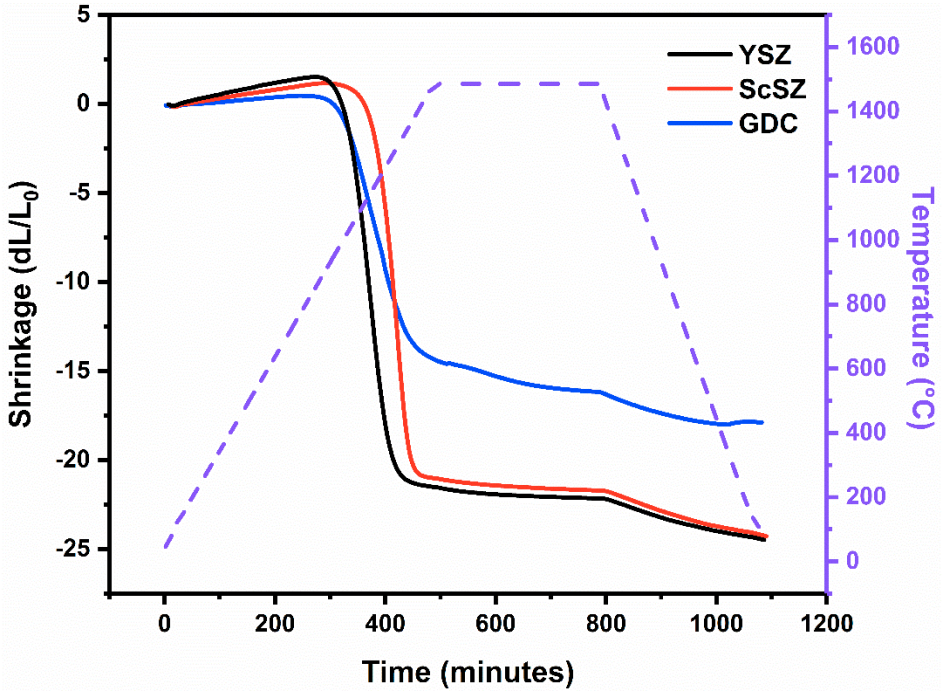

Figure 2: Dilatometry measurements for YSZ (black line), ScSZ (red line) and GDC (blue line)

4.3 Ceramic microstructures

Figure 3 shows the microstructure of polished and thermally etched surfaces of the sintered ceramics observed by SEM. All three ceramics have a highly dense microstructure. There are very few pores between the grains, in agreement with the high relative densities obtained by the Archimedes method, as shown in Table 4. The grain size distribution (calculated on around 1500 grains), shown in Figure 4, and the average grain size (AGS) are summarized in Table 4. As compared in Figure 4, GDC has narrower grain size distribution than YSZ and ScSZ. In addition to that, GDC has a much lower AGS (0.73 µm) than either ScSZ (2.97 µm) or YSZ (2.28 µm) (this is also the reason for the higher magnification of Figure 3 (c)). Therefore, in terms of total conductivity, GDC is expected to have a more significant contribution of grain boundary resistance compared to ScSZ and YSZ due to the larger amount of grain boundaries.

Furthermore, the highly dense microstructures shown here confirm that all three materials will have negligible effects of the porosity on the conductivity.

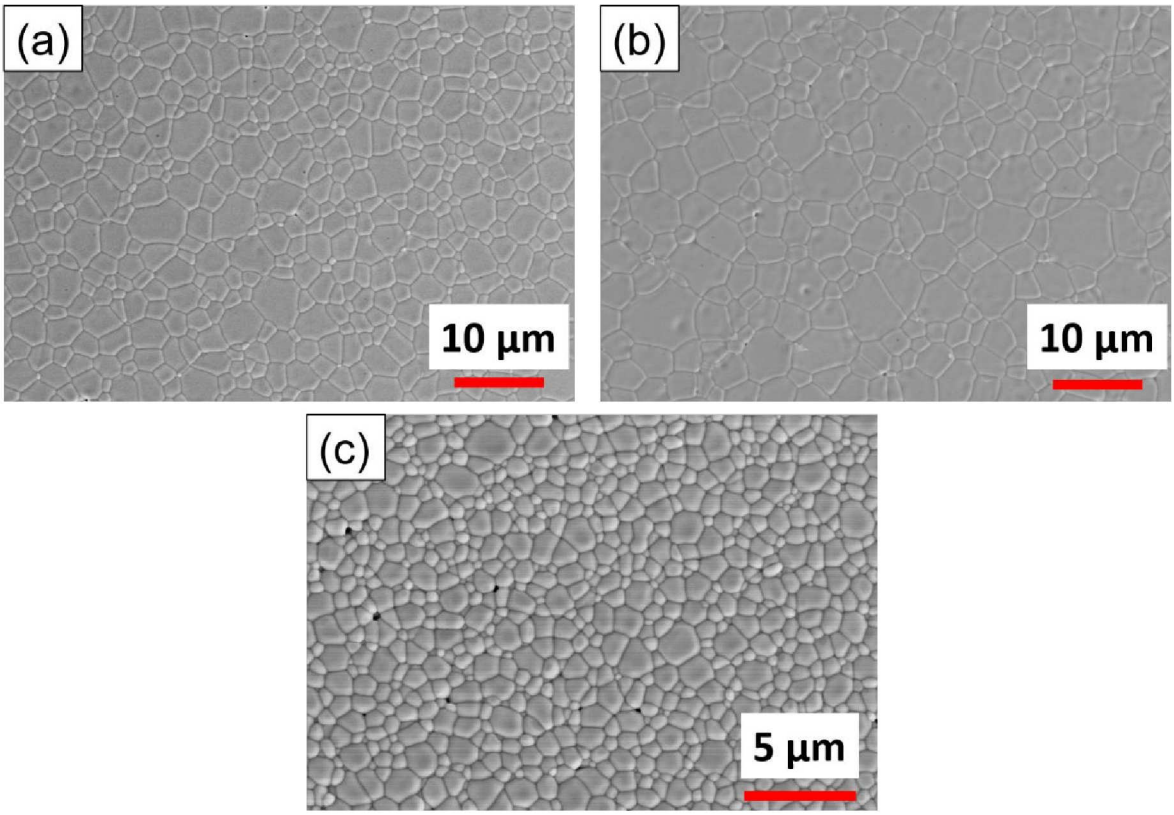

Figure 3 SEM images for (A) YSZ, (B) ScSZ, and (c) GDC

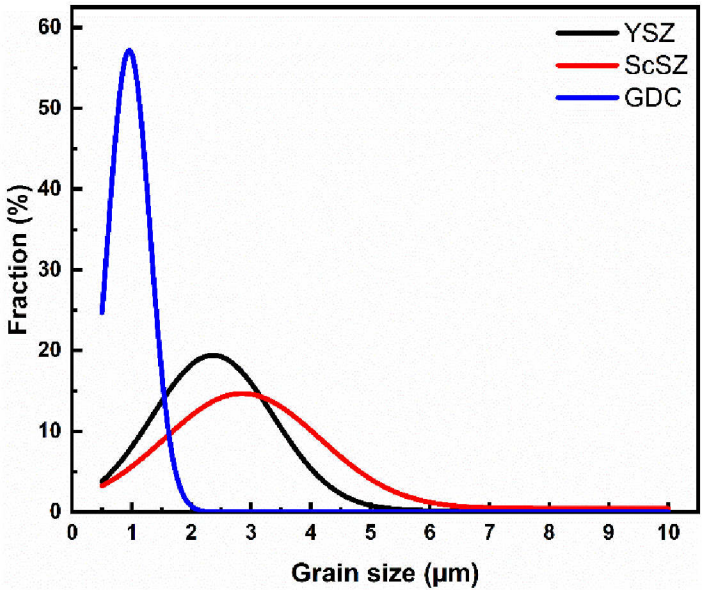

Figure 4 Grain size distribution for YSZ, ScSZ and GDC

Table 4 Comparison of relative green density and sintering density as well as the average grain size of the ceramics for YSZ, ScSZ and GDC

	YSZ	ScSZ	GDC
Relative green density (%)	45.3 ± 0.3	43.6 ± 0.4	57.2 ± 0.7
Relative sintering density (%)	98.9 ± 0.3	98.0 ± 0.1	97.9 ± 0.2
Average grain size (μm)	2.28 ± 1.0	2.97 ± 1.4	0.73 ± 0.3

4.4 EIS measurements

For an ion conducting ceramic with a thickness = L and an area = A, its total conductivity σ_{total} can be determined by:

$$\sigma_{total} = \frac{L}{R_{total}A} \tag{4}$$

where R_{total} is the total resistance of the ceramic, equaling to the sum of grain resistance R_b and grain boundary resistance R_{gb}. Since the EIS measurements were carried out under air atmosphere, all materials in this work are considered as pure oxide ionic conductors[37]. The conductivity of grain, σ_b, and grain boundary, σ_{gb}, is determined by:

$$\sigma_b = \frac{L}{R_b A} \tag{5}$$

$$\sigma_{gb} = \frac{C_b}{C_{gb}} \frac{L}{R_{gb} A} \tag{6}$$

where C_b and C_{gb} are the corresponding capacitances of grain and grain boundary, which serve as a geometrical correction for the much thinner GB than that for the grains, assuming that grains and grain boundaries have similar dielectric constants [57]. The EIS is then used to separate the grain and grain boundary resistances [58].

The recorded EIS for GDC, YSZ and ScSZ at 300 °C are shown in Figure 5. The inset of Figure 4 shows the equivalent circuit that was used to fit the data, with an *R-CPE* element representing the grain and grain boundary contributions, respectively. Here, a constant phase element (*CPE* with $Z = 1 / (j\omega Q)^{\alpha}$) is used for fitting instead of the capacitor (*C* with $Z = 1/j\omega C$). This is due to the fact that the semi-circle observed in Figure 4 is depressed, indicating a deviation from ideal capacitive behavior due to inhomogeneity in the system. The exponential factor α is close to unity (0.85—0.94, seen in Table 5), which is consistent with a slight deviation from ideal capacitive behavior (α = 1) [56]. The electrode response at low frequencies was excluded from the fit.

Then, the respective pseudo-capacitance *C* for each circuit is calculated from[59]:

$$C = (R^{1-\alpha}Q)^{\frac{1}{\alpha}} \tag{7}$$

The fitted parameters are listed in Table 5.

Base on the magnitude of capacitance C and characteristic frequency for each semicircle, the first semicircle at high frequencies is assigned to the grain response and the second one to the grain boundary response. Accordingly, R_1, R_2, C_1 and C_2 are assigned to the resistances and capacitances for grain and grain boundary as R_b, R_{gb}, C_b and C_{gb}, respectively. As can be found in Table 5, the capacitances for C_1 are in the range of 25—40 pF while the stray capacitance of the setup is 5 pF. The dielectric constants (or permittivity) ε_R (calculated from C_1 in the high frequency range and at 300 °C) for these three materials are also provided for comparison. The ε_R values in this work are in good agreement with reported values in literature. For example, for doped zirconia: Pimenov et al. [60] (ε_R = 63 – 86, 329 °C, ZrO_2-4 mol % Y_2O_3), Aigars et al. [61] (ε_R = 53, 300 °C, ZrO_2-7.5 mol % Y_2O_3) Boulouz et al. [62] (ε_R = 65.7, 300 °C, ZrO_2-8 mol % Y_2O_3), Tao et al. [63] (ε_R = 71, 340 °C, ZrO_2-8 mol % Sc_2O_3), and for doped ceria by Hiroshi et al. [64] (ε_R = 80 – 120, 300 °C, CeO_2-20 mol % Sm_2O_3), Ashok et al. [65] (ε_R = 14 – 102, 400 °C, CeO_2-15 mol % Gd_2O_3), Nowick et al [66] (ε_R = 25, 132.5 °C, 1 MHz, CeO_2-6 mol % Y_2O_3).

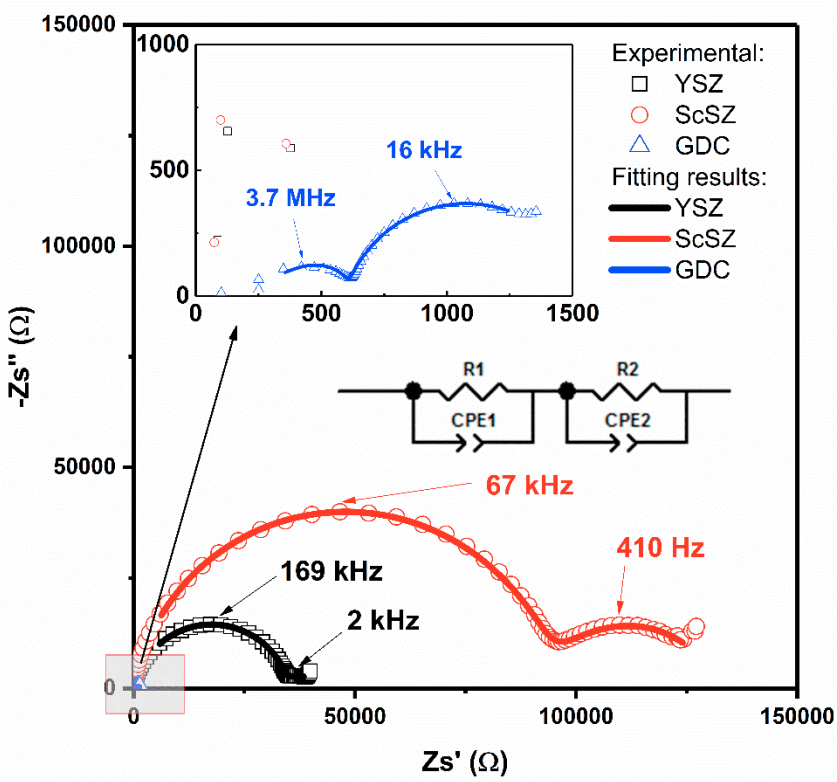

Figure 5 Typical impedance spectra of YSZ (black), ScSZ (red) and GDC (blue) at 300 °C. The experimental data are plotting in symbols and fitted data are plotting in lines.

Table 5 The fitted parameters for YSZ, ScSZ and GDC at 300 °C

	R_1 [Ω]	R_2 [Ω]	C_1 [F]	ε_r	C_2 [F]	Q_1 [F cm^{-1}]	α_1	Q_2 [F cm^{-1}]	α_2
YSZ	39456	4954	2.61×10^{-11}	66.3	2.63×10^{-8}	1.49×10^{-10}	0.87	5.65×10^{-8}	0.91
ScSZ	95207	34356	2.53×10^{-11}	68.5	1.38×10^{-8}	1.13×10^{-10}	0.88	4.38×10^{-8}	0.85

GDC	608	763	3.97×10^{-11}	47.9	1.11×10^{-8}	1.22×10^{-10}	0.94	5.74×10^{-8}	0.86

The Arrhenius plot of σ_b and σ_{gb} (the error bar for σ_{gb} considers the effects of stray capacitance on equation 6) for YSZ, ScSZ and GDC is shown in Figure 6. For all three electrolyte materials, the grain conductivity is always much higher than the grain boundary conductivity at all measured temperatures, consistent with [47]. However, some investigations found that the grain boundary conductivity is higher than the grain conductivity for Sc-doped zirconia, since the grain boundary semicircle is smaller than the grain semicircle in the impedance spectrum (indicating $R_b > R_{gb}$) [22, 67]. However, no geometrical correction was performed in those cases (equation (6)), so that the grain conductivity is compared to the grain boundary conductance.

The activation energy for the grain and grain boundary conductivity in the temperature range between 200 °C and 450 °C are listed in Table 6. For GDC and YSZ, the activation energy of the grain boundary conductivity is higher than that of the grain conductivity, which is consistent with other reports [47]. However, for ScSZ the activation energy of grain conductivity is higher than that of the grain boundary conductivity.

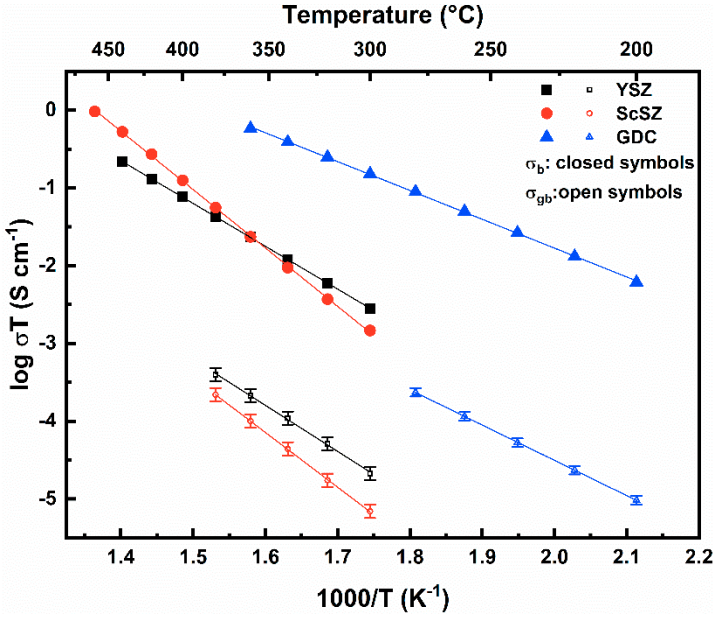

Figure 6 Comparison of bulk and grain boundary conductivity for YSZ (black), ScSZ (red) and GDC (blue), with open symbols standing for grain conductivity and closed symbols for bulk boundary conductivity

Table 6 List of activation energies of bulk and grain boundary for YSZ, ScSZ and GDC from 200—450 °C

samples	Activation energy (eV)	
	Bulk	Grain boundary
YSZ	1.09 ± 0.002	1.18 ± 0.022
ScSZ	1.49 ± 0.011	1.40 ± 0.009
GDC	0.74 ± 0.005	0.91 ± 0.003

Fehler! Verweisquelle konnte nicht gefunden werden. compares the total conductivities of YSZ, ScSZ and GDC from 300 °C to 800 °C. We can see that the ionic conductivity of GDC is not always higher than that of the zirconates. The conductivity of GDC is nearly the same as that of ScSZ at 600 °C (17.6 mS cm^{-1} vs 15.7 mS cm^{-1}) and even lower than that of ScSZ at temperatures higher than 650 °C. At lower temperatures (< 600 °C), GDC shows a higher ionic conductivity than both zirconates. Regarding ScSZ, though it has the highest ionic conductivity at temperatures higher than 650 °C, its ionic conductivity decreases significantly when lowering the temperature and is even lower than that of YSZ at temperatures below 400 °C.

As shown in Figure 7, the "two barrier model" can fit the experimental data very well. The four fitted parameters γ_1, γ_2, $E_{a,1}$, $E_{a,2}$ are listed in Table 7. The $E_{a,1}$ represents the high temperature activation energy and $E_{a,2}$ represents the low temperature activation energy. At low temperature, ScSZ has a higher activation energy than YSZ, and therefore a lower ionic conductivity than YSZ at temperatures below 400 °C. On the other hand, GDC shows a lower activation energy than either YSZ or ScSZ for the whole temperature range. Accordingly, the increase in ionic conductivity with temperature is less pronounced than for the zirconates. For comparison, the activation energy obtained by a simple linear fit using equation 2 (assuming there is only ''one barrier'' over the whole temperature range compared to the ''two barrier model'') is also included in Table 7. Using a single activation energy for fitting produces a value in between the two values obtained by the "two barrier model". This leads to progressively higher deviation at low and high temperatures, which is especially relevant when considering extrapolations made from such a one-barrier fit. The deviation between the two models at high temperature is 31.3%, 54% and 34.2% and XX%, YY% and ZZ% percent at low temperature for YSZ, ScSZ and GDC, respectively.

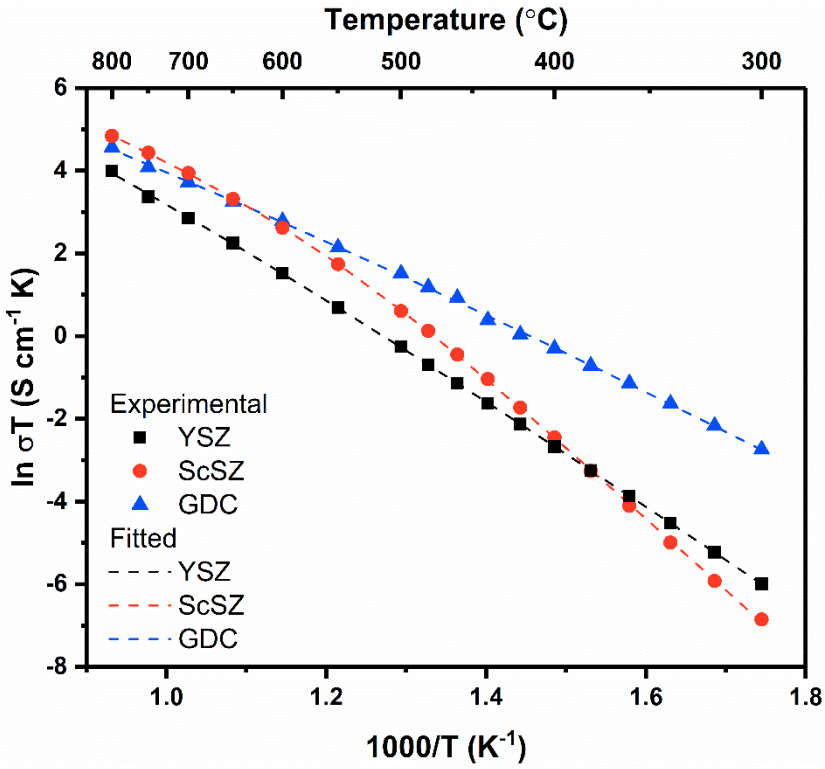

Figure 7 Comparison of experimental (denoted as symbols) and fitted plots (as dash lines) for YSZ (black), ScSZ (red) and GDC (blue) as a function of reciprocal temperature

Table 7 Fit parameters of conductivity data for YSZ, ScSZ and GDC using the two barrier model as well as a single barrier model from 300—800 °C

Materials	γ_1 [K S cm^{-1}]	γ_2 [K S cm^{-1}]	γ_1/γ_2	$E_{a,1}$ [eV]	$E_{a,2}$ [eV]	E [eV]
YSZ	5.26×10^5	2.54×10^7	48.3	0.80 ± 0.09	1.14 ± 0.03	1.05
ScSZ	3.55×10^5	1.6×10^{10}	45070	0.72 ± 0.03	1.50 ± 0.01	1.26
GDC	1.01×10^5	4.8×10^6	47.5	0.62 ± 0.06	0.89 ± 0.03	0.77

In Figure 8, we compare our measured ionic conductivity with the values reported in other dedicated conductivity studies for YSZ (Figure 8 (a)), ScSZ (Figure 8 (b)) and GDC (Figure 8 (c)). It should be pointed out here that the selected citations all have the same nominal composition as the materials used in this work. Since YSZ is an established electrolyte material for SOFC, the reported ionic conductivity values for YSZ are in quite good agreement with each other [56, 68, 69] (all the YSZ used in these literatures are commercial powder manufactured by TOSOH, Japan). However, some scatter exists for ScSZ and GDC. For ScSZ, our results agree well with other reported values [31, 70, 71]. But the reason for the lower ionic conductivity observed in [72] is not clear, which might be attributed to the microstructure (no detailed information is provided except a relative sintering density of 94%) or the impurity level of the raw powder (lab-synthesized ScSZ powder by Glycine-nitrate process and then ball milled). For GDC, our measured value also shows a good agreement with other reports [21, 73]. Though the microstructure reported in [74] is similar to ours, with average grain size of 1.22 µm and relative sintering density of 95% after

sintering at 1400 °C, their ionic conductivity is lower, where we assume the reason could be the lower gadolinium content caused by the polyol microwave assisted method they used for the synthesis of the powder.

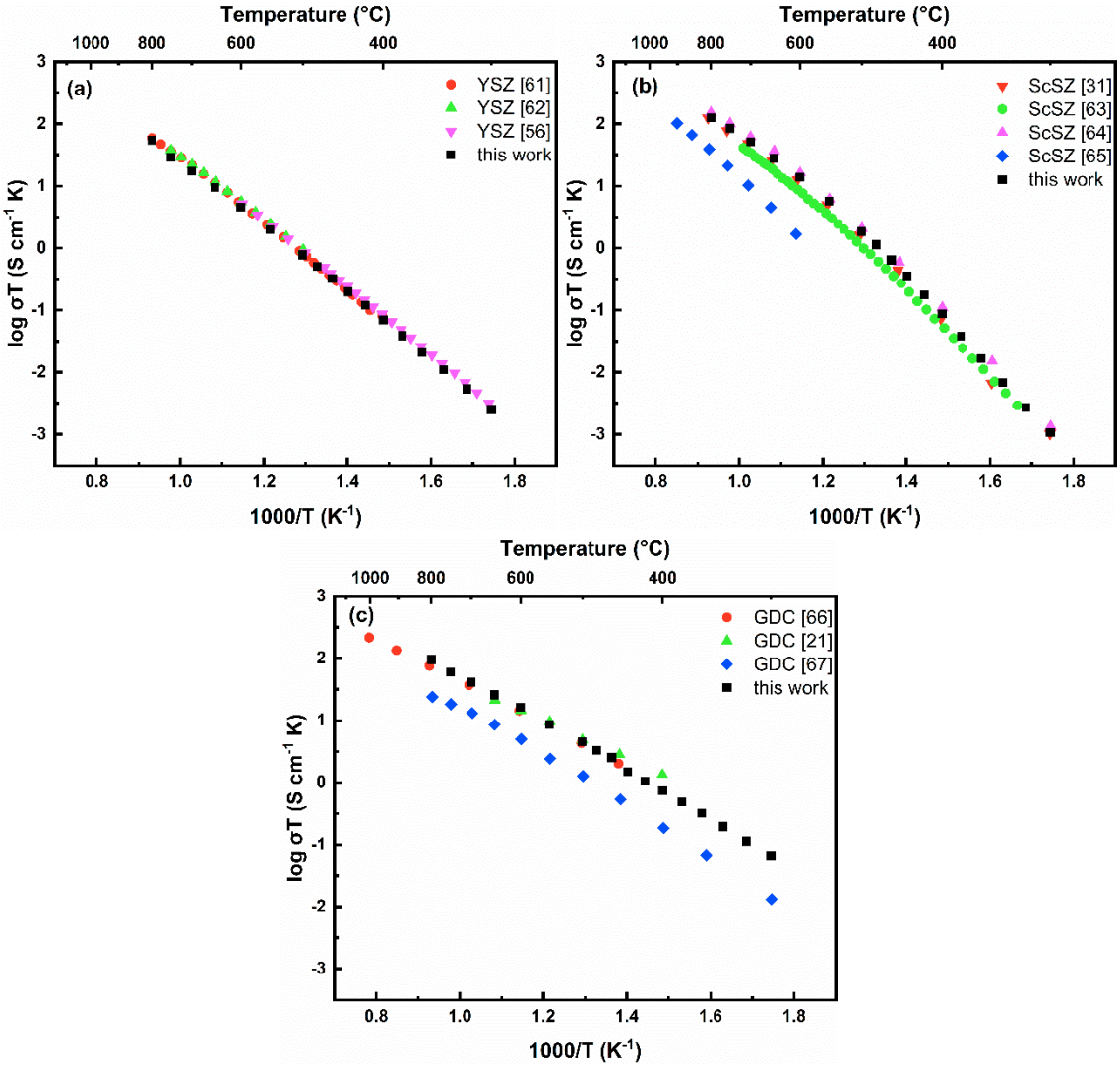

Figure 8 Ionic conductivity comparison with values in other reports for (a) YSZ (b) ScSZ (c) GDC

4.5 Grain size effects – a simple model

Due to their lower conductivity, the grain boundaries have a detrimental effect on the total ionic conductivity of a given electrolyte. Therefore, we are interested in the effect of the grain size on the total conductivity of an electrolyte of a given thickness. The idea is that a thin electrolyte consisting of only one single grain in the oxygen transport direction may show a different conductivity than predicted from conductivity values of a polycrystalline ceramic. To investigate the magnitude of the grain size effect, we consider the "brick layer" model [57] as shown in Figure 9:

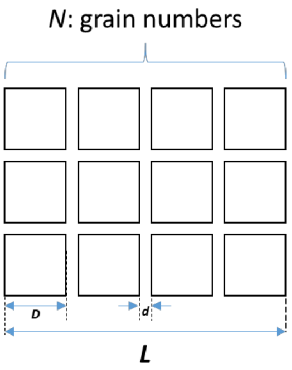

Figure 9 "Brick Layer" model of a polycrystalline material, with grain boundary thickness of *d*, grain size of *D*, sample thickness of *L* and grain number of *N*

For this simple model, we assume that the ceramic consists of identically shaped grains with a size *D* (that equals the average grain size of the real ceramic), which are separated by grain boundaries of thickness *d*. Then the area specific resistance (*ASR)* for such a polycrystalline material can be calculated as following:

$$ASR = \frac{L}{\sigma_{total}} = \frac{(N-1)d}{\sigma_{gb}} + \frac{ND}{\sigma_b} \tag{8}$$

The grain boundary thickness *d* can be calculated from[59]:

$$d = \frac{C_b}{C_{gb}} D \tag{9}$$

using the capacitance value in Table 5 and average grain size D in Table 4. A grain boundary thickness *d* of 2.3 ± 0.4 nm, 5.4 ± 1.0 nm and 2.6 ± 0.3 nm is derived for the studied YSZ, ScSZ and GDC, separately. As we see that $D \gg d$, therefore, $N \approx L/D$, we can further simplify equation (8) to:

$$ASR = \frac{d}{\sigma_{gb}}\left(\frac{L}{D} - 1\right) + L\frac{1}{\sigma_b} \tag{10}$$

The values of σ_b, σ_{gb} can be extrapolated from the values obtained by EIS (see Figure 6) to a temperature of 500 °C. We note that due to the non-linear behavior of the respective conductivity with temperature, extrapolation to higher temperatures shows a systematic deviation. Better input data is therefore required to apply this model at higher temperature. However, by assuming that the values of *d*, σ_b, σ_{gb}, C_{gb} and C_b are independent on the average grain size[59], we can plot the relationship between *ASR* and grain size *D* for different given electrolyte thicknesses at 500 °C, as shown in Figure 10 . The targeted *ASR* = 0.1 Ω·cm² is marked by a dashed line.

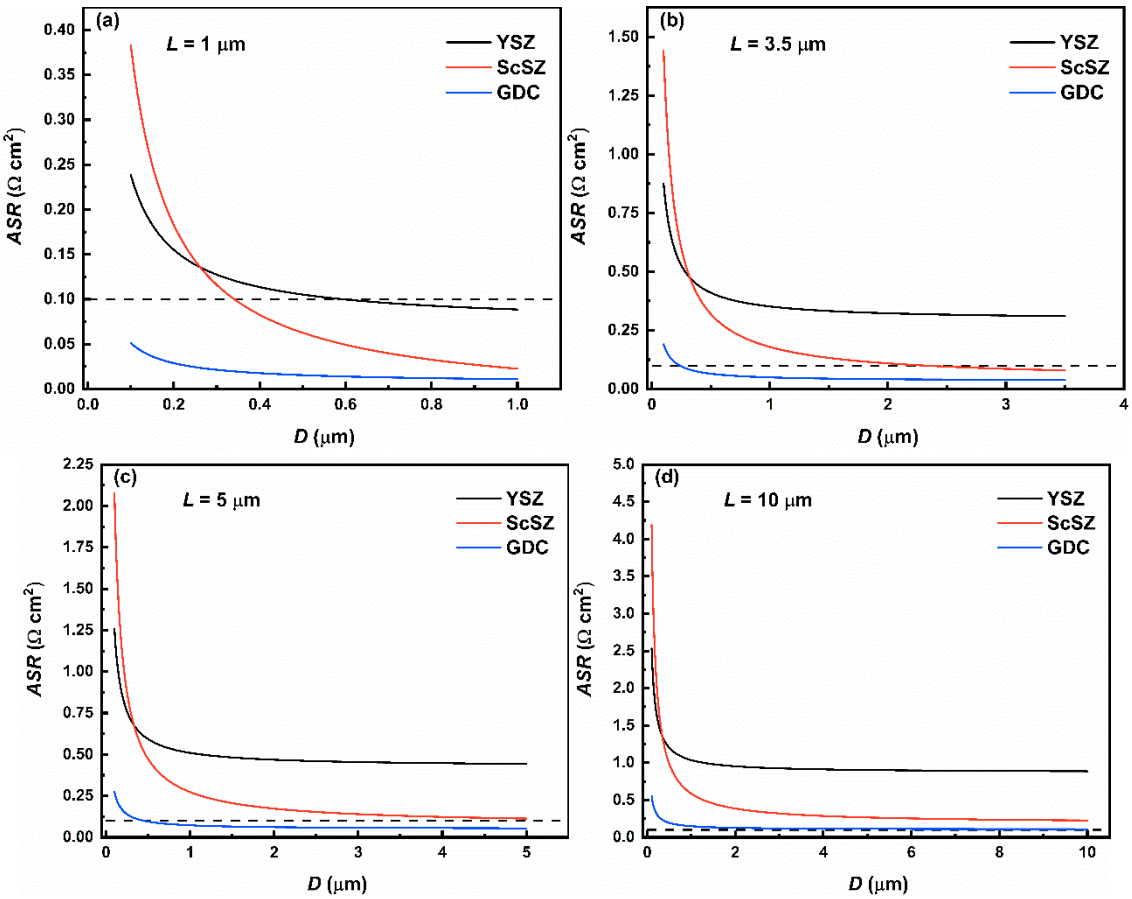

Figure 10 The dependence of ASR_{el} on the grain size for different fabricated electrolyte thickness *L* of (a): 1 µm, (b): 3.5 µm, (c): 5 µm and (d): 10 µm at 500 °C

Comparing Figure 10 (a), (b), (c) and (d), we see that using GDC might be easier and cheaper than YSZ and ScSZ in terms of electrolyte layer processing for reaching an *ASR* of electrolyte lower than 0.1 Ω cm^2 at 500 °C. For YSZ, the only possible way of using it at 500 °C is to fabricate an YSZ electrolyte as thin as 1 µm and at the same time, the average grain size along the ionic conducting pathway should not be smaller than 0.6 µm. While a thickness of 3.5 µm is needed for ScSZ, the average grain size along the ionic conducting pathway should not be smaller than 2.5 µm. On the other hand, a thickness of 5 µm with grain size not smaller than 0.5 µm is required for GDC, which could be achieved by scalable methods such as screen printing or tape casting. In addition, the compatibility of GDC with Sr- and Co-containing perovskite air electrodes means that the processing of GDC-based cells may be simplified compared to Zr-based electrolytes, which typically need a ceria-based barrier layer between the electrolyte and the air electrode.

5. Summary

In the face of some conflicting information about the ionic conductivities of GDC, ScSZ and YSZ in the literature, especially at low temperature (~ 500 °C), we compared the conductivities of dense ceramics made from well-defined, industrial-grade starting powders. We provide the information about the starting powder properties (including particle size distribution, powder morphology, impurity level and specific surface area), sintering behavior (dilatometry) and microstructure after sintering (density and average grain size). Evidently from the conductivity comparison which of the material that should be preferred

depends on the temperature. In the traditional high temperature range (> 700 °C), thin YSZ can still be viewed as the first choice for the electrolyte material for SOFC. While at much lower temperature (< 500 °C), GDC seems to be the best potential electrolyte material due to its superior ionic conductivity. Using a simple "brick layer" model, we show that the grain size is relevant for the prediction of ASR values. This tool gives us to the possibility to predict the influence of the microstructure of a thin, supported electrolyte on its conductance, and allows the targeted design of electrolyte microstructure.

Acknowledgement

The Chinese Scholarship Council (CSC) is highly appreciated for its financial support for Jun Zhang's study in Forschungszentrum Jülich. The authors thank: Dr. Chih-Long Tsai for the fruitful discussions with EIS and proofread of the manuscript, Dr. Doris Sebold for the SEM images observation and Dr. Robert Mücke for the guidance of brick model interpretation (all from IEK-1 in Forschungszentrum Jülich).

Reference

[1] F. Han, R. Mücke, T. Van Gestel, A. Leonide, N.H. Menzler, H.P. Buchkremer, D. Stöver, *J. Power Sources* **218** (2012) 157.
[2] L. Blum, L.G.J. de Haart, J. Malzbender, N. Margaritis, N.H. Menzler, *Energy Technology* **4** (2016) (8) 939.
[3] A. Mai, J.A. Schuler, F. Fleischhauer, V. Nerlich, A. Schuler, *ECS Transactions* **68** (2015) (1) 109.
[4] B.P. Borglum, H. Ghezel-Ayagh, *ECS Transactions* **68** (2015) (1) 89.
[5] E.D. Wachsman, K.T. Lee, *Science* **334** (2011) (6058) 935.
[6] R. Küngas, S. Veltzé, S. Ovtar, Y. Xu, S.B. Simonsen, K. Kwok, H.L. Frandsen, A. Samson, P. Zielke, W.-R. Kiebach, Long-Term Stability of Anode-Supported Solid Oxide Fuel Cells with a Co-Sintered Cathode Backbone and Infiltrated La0. 95Co0. 4Ni0. 6O3 (LCN) Electro-Catalyst, *Meeting Abstracts*, The Electrochemical Society (2016), p.2895-2895.
[7] T.L. Skafte, J. Hjelm, P. Blennow, C.R. Graves, Quantitative review of degradation and lifetime of solid oxide cells and stacks, *12th European SOFC & SOE Forum*, European Fuel Cell Forum (2016).
[8] N. Margaritis, L. Blum, P. Batfalsky, D. Bohmann, S. Ceschini, Q. Fang, D. Federmann, J. Kroemer, R. Peters, R. Steinberger-Wilckens, *ECS Transactions* **68** (2015) (1) 209.
[9] D.J.L. Brett, A. Atkinson, N.P. Brandon, S.J. Skinner, *Chem. Soc. Rev.* **37** (2008) (8) 1568.
[10] B.C.H. Steele, A. Heinzel, *Nature* **414** (2001) (6861) 345.
[11] B.C.H. Steele, *J. Power Sources* **49** (1994) (1-3) 1.
[12] J.M. Vohs, R.J. Gorte, *Adv. Mater.* **21** (2009) (9) 943.
[13] Z. Gao, L.V. Mogni, E.C. Miller, J.G. Railsback, S.A. Barnett, *Energy & Environmental Science* **9** (2016) (5) 1602.
[14] J. Will, A. Mitterdorfer, C. Kleinlogel, D. Perednis, L.J. Gauckler, *Solid State Ionics* **131** (2000) (1-2) 79.
[15] D.Y. Jang, M. Kim, J.W. Kim, K. Bae, J.-w. Son, M.V.F. Schlupp, J.H. Shim, *J. Electrochem. Soc.* **164** (2017) (6) F484.
[16] Z. Lu, J. Hardy, J. Templeton, J. Stevenson, D. Fisher, N. Wu, A. Ignatiev, *J. Power Sources* **210** (2012) 292.
[17] R. Nédélec, S. Uhlenbruck, D. Sebold, V.A.C. Haanappel, H.P. Buchkremer, D. Stöver, *J. Power Sources* **205** (2012) 157.
[18] T. Van Gestel, D. Sebold, H.P. Buchkremer, *J. Eur. Ceram. Soc.* **35** (2015) (5) 1505.

[19] T.-H. Yeh, W.-C. Hsu, C.-C. Chou, *Journal de Physique IV (Proceedings)* **128** (2005) 213.
[20] D.W. Jung, K.L. Duncan, E.D. Wachsman, *Acta Mater.* **58** (2010) (2) 355.
[21] C. Xia, M. Liu, *Solid State Ionics* **152-153** (2002) 423.
[22] A. Kumar, A. Jaiswal, M. Sanbui, S. Omar, *J. Am. Ceram. Soc.* **100** (2017) (2) 659.
[23] T. Ishihara, H. Matsuda, Y. Takita, *J. Am. Chem. Soc.* **116** (1994) (9) 3801.
[24] O. Yamamoto, *Electrochim. Acta* **45** (2000) (15-16) 2423.
[25] S. Sanna, V. Esposito, J.W. Andreasen, J. Hjelm, W. Zhang, T. Kasama, S.B. Simonsen, M. Christensen, S. Linderoth, N. Pryds, *Nature Materials* **14** (2015) (5) 500.
[26] P. Shuk, H.D. Wiemhöfer, U. Guth, W. Göpel, M. Greenblatt, *Solid State Ionics* **89** (1996) (3) 179.
[27] K. Huang, M. Feng, J.B. Goodenough, *J. Electrochem. Soc.* **144** (1997) (10) 3620.
[28] R. Doshi, V.L. Richards, J.D. Carter, X. Wang, M. Krumpelt, *J. Electrochem. Soc.* **146** (1999) (4) 1273.
[29] C. Xia, M. Liu, *Solid State Ionics* **144** (2001) (3-4) 249.
[30] B.C.H. Steele, *Solid State Ionics* **129** (2000) (1-4) 95.
[31] D.-S. Lee, W.S. Kim, S.H. Choi, J. Kim, H.-W. Lee, J.-H. Lee, *Solid State Ionics* **176** (2005) (1-2) 33.
[32] A. Kumar, A. Jaiswal, M. Sanbui, S. Omar, *Scripta Mater.* **121** (2016) 10.
[33] M. Shimazu, K. Yamaji, H. Kishimoto, A. Ueno, T. Isobe, K.-i. Katsumata, H. Yokokawa, K. Okada, *Solid State Ionics* **224** (2012) 6.
[34] M. Shimazu, T. Isobe, S. Ando, K.-i. Hiwatashi, A. Ueno, K. Yamaji, H. Kishimoto, H. Yokokawa, A. Nakajima, K. Okada, *Solid State Ionics* **182** (2011) (1) 120.
[35] Y. Zhang, R. Knibbe, J. Sunarso, Y. Zhong, W. Zhou, Z. Shao, Z. Zhu, *Adv. Mater.* **29** (2017) (48).
[36] J.W. Fergus, *J. Power Sources* **162** (2006) (1) 30.
[37] V.V. Kharton, F.M.B. Marques, A. Atkinson, *Solid State Ionics* **174** (2004) (1-4) 135.
[38] L. Malavasi, C.A.J. Fisher, M.S. Islam, *Chem. Soc. Rev.* **39** (2010) (11) 4370.
[39] O. Bohnke, V. Gunes, K.V. Kravchyk, A.G. Belous, O.Z. Yanchevskii, O.I. V'Yunov, *Solid State Ionics* **262** (2014) 517.
[40] W. Sun, N. Zhang, Y. Mao, K. Sun, *J. Power Sources* **218** (2012) 352.
[41] N. Mahato, A. Banerjee, A. Gupta, S. Omar, K. Balani, *Prog. Mater Sci.* **72** (2015) 141.
[42] J.A. Kilner, M. Burriel, *Annual Review of Materials Research* **44** (2014) (1) 365.
[43] K.C. Wincewicz, J.S. Cooper, *J. Power Sources* **140** (2005) (2) 280.
[44] S.C. Singhal, *Solid State Ionics* **152-153** (2002) 405.
[45] T. Mori, Y. Wang, J. Drennan, G. Auchterlonie, J.-G. Li, T. Ikegami, *Solid State Ionics* **175** (2004) (1-4) 641.
[46] X.J. Chen, K.A. Khor, S.H. Chan, L.G. Yu, *Materials Science and Engineering: A* **335** (2002) (1-2) 246.
[47] X. Guo, R. Waser, *Prog. Mater Sci.* **51** (2006) (2) 151.
[48] H.A. Abbas, C. Argirusis, M. Kilo, H.-D. Wiemhöfer, F.F. Hammad, Z.M. Hanafi, *Solid State Ionics* **184** (2011) (1) 6.
[49] N. Jiang, E.D. Wachsman, S.-H. Jung, *Solid State Ionics* **150** (2002) (3-4) 347.
[50] J.A. Kilner, B.C.H. Steele, In: O.T. Sørensen, Editor, *Nonstoichiometric Oxides*, Academic Press (1981), p.233-269.
[51] T.I. Politova, J.T.S. Irvine, *Solid State Ionics* **168** (2004) (1-2) 153.
[52] G.M. Rupp, M. Glowacki, J. Fleig, *Journal of The Electrochemical Society* **163** (2016) (10) F1189.
[53] S.P.S. Badwal, *Journal of Materials Science* **19** (1984) (6) 1767.
[54] Z. Zhan, T.-L. Wen, H. Tu, Z.-Y. Lu *Journal of The Electrochemical Society* **148** (2001) (5) A427.
[55] A.S. Nowick, D.S. Park, In: G.D. Mahan, W.L. Roth, Editors, *Superionic Conductors*, Springer US, Boston, MA (1976), p.395-412.
[56] C. Ahamer, A.K. Opitz, G.M. Rupp, J. Fleig, *J. Electrochem. Soc.* **164** (2017) (7) F790.

[57] S.M. Haile, D.L. West, J. Campbell, *J. Mater. Res.* **13** (2011) (06) 1576.
[58] J.T.S. Irvine, D.C. Sinclair, A.R. West, *Adv. Mater.* **2** (1990) (3) 132.
[59] C. Peters, A. Weber, B. Butz, D. Gerthsen, E. Ivers-Tiffée, *J. Am. Ceram. Soc.* **92** (2009) (9) 2017.
[60] A. Pimenov, J. Ullrich, P. Lunkenheimer, A. Loidl, C. Rüscher, *Solid State Ionics* **109** (1998) (1-2) 111.
[61] A. Vītiņš, *J. Solid State Electrochem.* **5** (2001) (7-8) 479.
[62] M. Boulouz, F. Tcheliebou, A. Boyer, *J. Eur. Ceram. Soc.* **17** (1997) (14) 1741.
[63] J. Tao, A. Dong, J. Wang, *Materials Transactions* **54** (2013) (5) 825.
[64] H. Yamamura, S. Takeda, K. Kakinuma, *Solid State Ionics* **178** (2007) (13-14) 889.
[65] A. Kumar Baral, V. Sankaranarayanan, (2010).
[66] A. Nowick, A. Vaysleyb, I. Kuskovsky, *Physical Review B* **58** (1998) (13) 8398.
[67] S. Omar, W. Bin Najib, W. Chen, N. Bonanos, B. Dunn, *J. Am. Ceram. Soc.* **95** (2012) (6) 1965.
[68] F. Ciacchi, K. Crane, S. Badwal, *Solid State Ionics* **73** (1994) (1-2) 49.
[69] X. Guo, E. Vasco, S. Mi, K. Szot, E. Wachsman, R. Waser, *Acta Mater.* **53** (2005) (19) 5161.
[70] Z. Wang, M. Cheng, Z. Bi, Y. Dong, H. Zhang, J. Zhang, Z. Feng, C. Li, *Mater. Lett.* **59** (2005) (19-20) 2579.
[71] J. Tan, Y. Su, T. Hu, Q. Yu, R. Tursun, Q. Li, Y. Xi, *Solid State Ionics* **292** (2016) 22.
[72] H.P. Dasari, J.S. Ahn, K. Ahn, S.-Y. Park, J. Hong, H. Kim, K.J. Yoon, J.-W. Son, H.-W. Lee, J.-H. Lee, *Solid State Ionics* **263** (2014) 103.
[73] S. Wang, T. Kobayashi, M. Dokiya, T. Hashimoto, *J. Electrochem. Soc.* **147** (2000) (10) 3606.
[74] M.A.F. Öksüzömer, G. Dönmez, V. Sariboğa, T.G. Altinçekiç, *Ceram. Int.* **39** (2013) (7) 7305.